A plasma electrochemistry reactor for the synthesis of radioactive gold nanoparticles

S. Turgeon[*], M. Bouchard[*, **, ***], M. Laprise-Pelletier[*, **, ***] and M.A. Fortin[*, **, ***]

[*] Axe médecine régénératrice, Centre hospitalier universitaire (CHU) de Québec, 10 rue de l'Espinay, Québec, G1L 3L5, Canada

[**] Département de génie des mines, de la métallurgie et des matériaux, Université Laval, Québec, G1V 0A6, Canada

[***] Centre de recherche sur les matériaux avancés (CERMA), Université Laval, Québec, G1V 0A6, Canada

ABSTRACT

Radioactive gold nanoparticles (^{198}Au:Au NPs) are being considered as substitutes for the massive seeds currently used in prostate cancer brachytherapy. However, their therapeutic use is hindered by the short half-life of ^{198}Au (2.7 days) combined to the difficulty to adapt conventional colloidal nanoparticles synthesis techniques to fully comply with radioprotection requirements. Here we present a plasma-based process which is portable, automatable and which involves relatively little manipulation. It is therefore compatible with the in-situ, on-demand synthesis of therapeutic ^{198}Au-doped nanoparticles. Highly efficient nanoparticles synthesis is demonstrated for both stable (Au) and radioactive (^{198}Au) gold.

Keywords: radioactive gold nanoparticles, plasma electrochemistry, dielectric barrier discharge, *in situ* spectroscopy, atmospheric pressure plasma

1 INTRODUCTION

Gold nanoparticles doped with the ^{198}Au isotope (β emission of 0.96 MeV, average γ of 412 keV, half-life of 2.7 days), directly injected in prostate cancer tumors, has recently been proposed as an alternative to macroscopic seeds containing ^{125}I or ^{103}Pd. These seeds represent a common internal radiotherapy (brachytherapy) treatment of prostate cancer. Nanometric-sized sources could provide a more precise, less invasive and more uniform dose-delivery treatment. Indeed, Shukla *et al.* [1] have measured an 80% volume reduction of tumors 28 days after a single intra-tumoral injection of ^{198}Au-doped nanoparticles in human prostate cancer-bearing mice, demonstrating the therapeutic efficiency of these nanoparticles.

Yet, the synthesis of nanoparticles that are radioactive, short-lived and dedicated to injection in humans is very constraining, particularly if it is to be performed close to the clinical setting. The process must be quick, should imply a very limited number of manipulations (radioprotection issues) on relatively small volumes of aqueous fluid. The process should be efficient and ideally fully automated. All this exludes most if not all the conventional chemical and thermal nanoparticle synthesis processes.

Recently-introduced atmospheric pressure plasma electrochemistry brings a promising alternative. A plasma is a partly-ionised gas; it can be generated between an upper conductive electrode and the surface of a solution to be treated. Essentialy, a gaz such as argon flowing over the aqueous solution of gold (or another noble metal) salt is partially ionised by an electric field, becoming a plasma. The plasma is composed of electrons as well as positive ions, and excited atoms of argon, oxygen and nitrogen (O and N species present in residual concentrations). Electrons can in principle directly reduce the gold ions into metallic nanoparticles near the surface of the solution; however, recent results point to a more complex process involving dissolved reactive species produced by the interactions between the different species present in the plasma and the liquid.

One of the first such reactor used for the synthesis of nanoparticles was based on the micro-hollow cathode principle. Such a setup is particularly easy and inexpensive to build and to operate. It is however limited to ultra-small productions, even in the multi-cathode configuration [2]. it also raises issues related to purity control. The dielectric barrier discharge (DBD) type of reactor is much more adapted to the treatment of large surfaces of fluids (and to larger volumes), and to the preservation of high purities.

The present work is based on a newly developed DBD reactor configured for the treament of continuously-flowing solutions of widely variable volume with in situ, realtime monitoring of the process by ultraviolet-visible (UV-Vis) absorbance spectroscopy.

2 MATERIALS AND METHODS

2.1 Plasma synthesis equipment and in situ spectroscopy

The main characteristics of the DBD reactor that was used for the synthesis of both stable Au nanoparticles and ^{198}Au-doped nanoparticles, are described here. The gold salt solution is circulated by an external pump through a long and narrow (~1 cm) channel, then through an in-line quartz spectroscopy cell (Spectrosil Quartz, Starna Cells). Argon gas (99.999%, Linde Canada) is flown perpendicularly through a small gap (~3 mm) over the

channel. It is ionized by an alternating electric field applied from above (7.5 kV peak, 25 kHz) through a quartz dielectric barrier. The gold solution is electrically grounded by a corrosion-resistant electrode situated away from the discharge. The configuration and materials are optimised for high purity, efficient heat management, and easy replacement of worn or contaminated parts. The UV-Vis absobance of the outflowing solution/suspension is measured with a fiber optic-coupled UV-Vis spectrometer (HR4000CG-UV-NIR, Ocean Optics). For a more detailed description of the reactor design, the reader is refered to paper 876 of the present proceedings.

2.2 Preparation of gold ions precursors

Trihydrated chlorauric acid ($HAuCl_4 \cdot 3\ H_2O$, Sigma-Aldrich) and ($H^{198}AuCl_4$, ~500 µCi, Research Reactor Center, University of Missouri-Columbia) precursors were of purity > 99%, and were used as is. Nanopure water (20 mL, Barnstead, 18.2 MΩ) was used to dissolve the metal ion precursors to a concentration of 1 mM. This solution was supplemented with dextran (M.W. 5 kDa, Carbomer Inc.) at 0.2 mM, used as steric stabilizer during the nanoparticles growth. For the synthesis of radioactive nanoparticles, 20 µL of ^{198}Au was added to the solution described above.

2.3 Nanoparticle plasma synthesis procedure: in situ monitoring profile

The synthesis procedure was as follows. The 20 mL of solution was closed-loop circulated through the system for the entire period of treatment which correponded to the duration of application of the high, alternating voltage (7.5 kV amplitude, 25 kHz frequency). The treatment was fixed to 30 min unless othewise noted. Meanwhile, 100 mL/min of argon was flowing through the discharge gap.

UV-Vis absorbance spectra were acquired at regular intervals of time (typically 5 s) over the 400 nm to 800 nm wavelenght range for the observation of the surface plasmon resonnance (SPR) peak which is strictly related to the presence of gold nanoparticles (figure 1). Otherwise, spectra could be acquired over the 200 nm to 400 nm wavelenght range for the observation of the peak related to gold ions. The evolution of these two peaks is anti-correlated, and indicates the amount of reduction of the solvated ions into metallic nanoparticles.

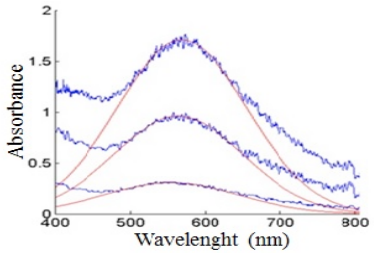

Figure 1: UV-vis spectra of the surface plasmon resonance (SPR) peak at different times.

2.4 Analytical methods

POST-SYNTHESIS UV-VIS SPECTROSCOPY

After plasma synthesis, 1 mL of the suspension was analyzed by ex-situ UV-Vis absorbance spectral measurements (200 to 800 nm, UV-1601, Shimadzu) in a quartz cell (path length: 10 mm), in order to follow the stability of the nanoparticles suspensions over time.

SIZE MEASUREMENTS (DLS, TEM)

The hydrodynamic diameters of diluted nanoparticles suspensions in water (1/10) were evaluated by dynamic light scattering (DLS; Malvern Zetasizer, 173°), at 25° C from the average of three measurements. The viscosity and refractive index of water were set to 0.8872 cp and 1.33 respectively. For the gold nanoparticles, the refractive index was set to 0.2. Size distributions of the metallic cores were evaluated based on images obtained by transmission electron microscopy (120 keV, TEM; FEI Tecnai Spirit Biotwin, FEI Company), after deposition of diluted suspension drops on carbon-coated copper grids (300 mesh, Electron Microscopy Sciences). Images were analysed with the Image J software.

PURIFICATION AND QUANTIFICATION

In order to eliminate the remaining free $AuCl_4^-$ ions and dextran molecules from the plasma treated solution of ^{198}Au doped nanoparticles, a centrifugation step was performed in a 50 mL tube containing a centrifugal filter (30 kDa pores, Amicon Ultra-15, Merck Millipore Ltd) for 30 min at 1000 x g. Three types of suspensions/solution were then obtained: large nanoparticles (L-NPs), small nanoparticles (S-NPs) as well as solvated ions and dextran.

For non-radioactive samples, the gold concentration of the solution of residual ions was measured by microwave plasma atomic emission spectroscopy (MP-AES 4100, upgraded to 4200) after digestion at 115°C in aqua regia and H_2O_2 (30%, Sigma-Aldrich).

For the ^{198}Au doped samples, radioactivity measurements were conducted for each type of suspension/solution mentioned above using an Atomlab 100 dose calibrator (Biodex Medical systems).

3 RESULTS AND DISCUSSION

Different conditions have been tested with non-radioactive gold in order to determine the optimal set of parameters for the synthesis of nanoparticles most suited for cellular integration and radiotherapeutic effect. The ratio of the dextran/gold concentrations was of particular importance. Only the final selection will be discussed here: 1 mM of $HAuCl_4$ and 0.2 mM of Dextran; discharge duration of 30 min; 7.5 kV, 25 kHz applied voltage.

The particles obtained were visualized by TEM as shown in figure 2a. Image analysis lead to their mean sphericity which is superior to 0.8 and to their size distribution shown in figure 2b which is unimodal and relatively narrow with 98% of the particles within the range

of 10 to 50 nm. The particles are therefore small enough to minimize auto-attenuation of their emissions and large enough to prevent lymphatic drainage. Their sphericity also favors their tumor uptake [3].

Figure 2c shows the hydrodynamic size distribution of the particles in aqueous suspension, measured by DLS. The features are the same although the size scale is shifted towards higher values, as expected for DLS measurements (includes the molecular and electrostatic corona around the particles). Following a synthesis, the remaining concentration of gold salts was measured by AES elementary analyses. The concentration obtained was 1.9 ± 0.6 µM of the initial 1 mM leading to a reduction yield of 99.8 ± 0.1 %. This figure is much higher than what can be obtained through thermal reduction in otherwise similar conditions [4].

The stability of such a fully-reduced nanoparticles suspension has then been evaluated by comparing DLS and UV-VIS absorbance analyses on as-synthesised and 7-day aged samples. The hydrodynamic size distribution (figure 3a) remained almost unchanged. The slight shift of the main DLS peak (from 77 to 80 nm) is likely due to a reorganisation of the dextran chains at the nanoparticles' surface. The shift of the smaller peak (from 7 to 9.5 nm) is likely due to dextran aggregates since almost no Au nanoparticles of such size could be observed by TEM. The surface plasmon resonance peak which can be observed around 530 nm on figure 3b, as well as the ion-related region of the absorbance spectra close to 300 nm, remained quasi-identical. The combined results indicate a complete stability of the samples in terms of suspension, size distribution and concentration.

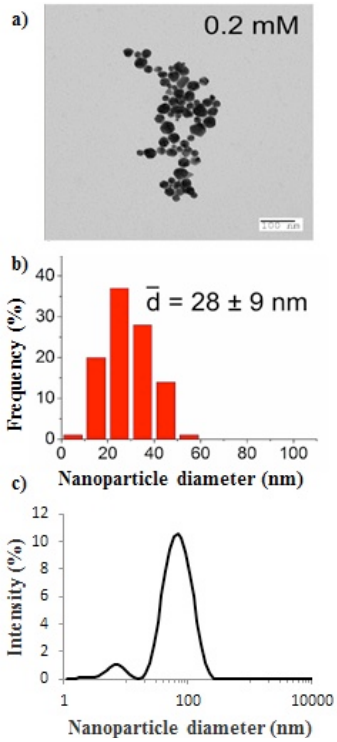

Figure 2: a) TEM image of Au nanoparticles synthesized by DBD plasma with dextran b) corresponding size distribution; c) intensity-weighted DLS size distribution

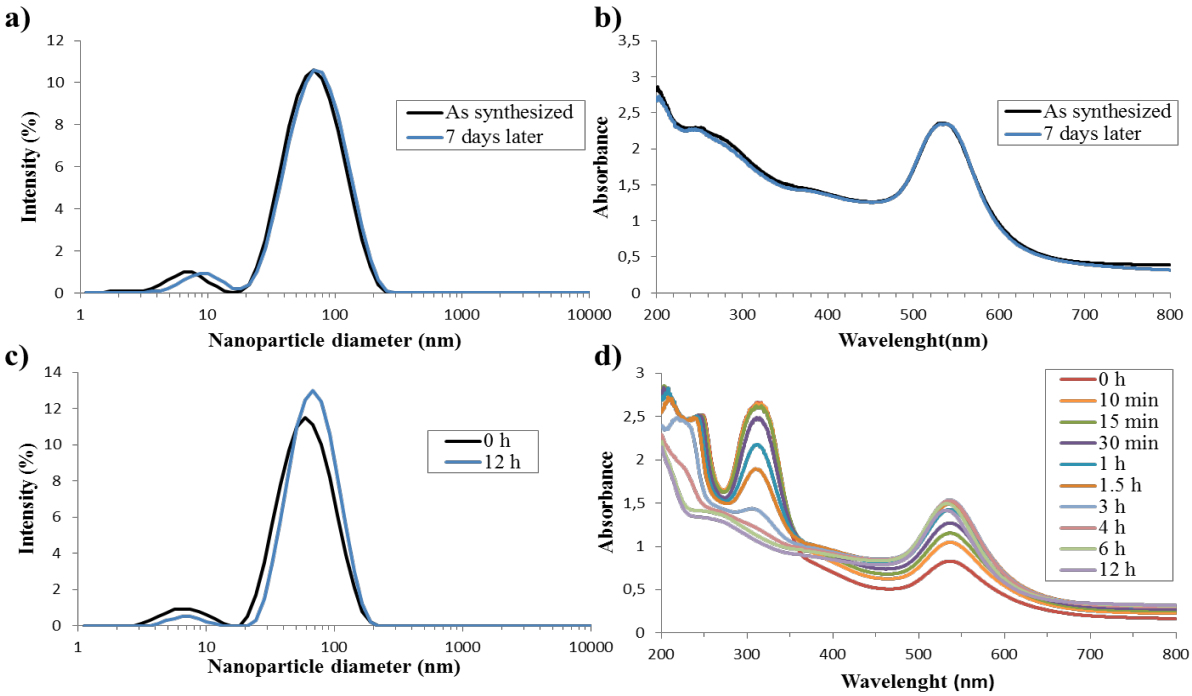

Figure 4: Stability of Au nanoparticles suspensions; a) hydrodynamic size distributions of fully plasma-reduced suspensions b) corresponding UV-visible absorbance spectra; c) partially reduced nanoparticles; d) corresponding UV-visible spectra.

Partially reduced solutions/suspensions proved to behave differently however. The stability of a solution treated for only 5 min was evaluated as above-mentionned over a period of 12 hours. The results, shown of figure 3c and 3d indicate that reduction continues for hours after the treatment. The DLS peak shifts slightly towards higher sizes indicating an increase of particle size , however little agglomeration. The $AuCl_4^-$-related absorbance peak decreases continuously over the entire period. Meanwhile, the SPR absorbance peak increases for 4 hours, then decreases. This indicates that while the reduction process is still ongoing, some sedimentation of the largest particles occurs which furthermore could be visually observed at the bottom of the quartz cell. Agglomerated particles, if present, are therefore sedimented and accordingly do not appear in the DLS curve. Nevertheless, the resulting auto-reduced suspension is unstable unlike the suspension fully reduced by plasma.

Preparation and characterisation of radioactive nanoparticles had to be performed somewhat differently due to safety issues. The solution was prepared by the adition of 20 µL of $^{198}AuCl_4^-$ solution (approximately 500 µCi) to a "standard" 20 mL solution. It was then plasma-treated for 30 min.

Size evaluation had to be simplified and was based on centrifugal separation in two sub-populations of Large (>~38 nm) and Small (<~38 nm) nanoparticles as well as remaining solution. TEM images (figure 4) were performed on very small quantities of largely (radioactively) decayed samples of both sub-populations. Their size distributions are consistent with what was obtained for non-radioactive particles, except for the presence of a somewhat larger fraction of Large ones (> 50 nm). This effect could be due to the influence of the very acidic $H^{198}AuCl_4$ solution (pH < 0.5).

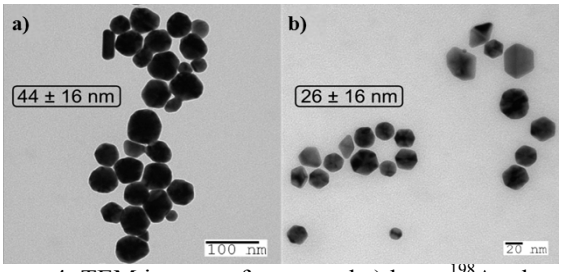

Figure 4: TEM images of separated a) large ^{198}Au doped nanoparticles; b) small ^{198}Au doped nanoparticles.

Dosimetry measurements directly lead to the fraction of the ^{198}Au atoms that were included in the Large and the Small naoparticles and in the remaining unreduced salts. The results immediately after the synthesis were 22±4%, 34±1% and 44±3% respectively. The initial reduction efficiency was therefore 56% significantly lower to what could be expected from the non-radioactive experiments i.e. 99.8%. This could again be due to the very acidic $H^{198}AuCl_4$ solution, that can affect Au nanoparticle size.[5, 6].

The more acid radioactive gold has an evident impact on nanoparticle growth. However, an obvious solution to this was inspired by the non-radioactive experiments: auto-reduction over many hours. Hence, an as-synthesized solution was left for for 16 hours and then separated in the two sub-populations (L-NP and S-NP) plus remaining solution. The radioactivity of each fraction was then measured: 94±1%, 6±1% and <0.1% respectively for the L-NP, S-NP, and remaining ions solutions. The final reducing efficiency therefore reached as high a level as for the non-radioactive syntheses, only by leaving the suspensions for ageing at room temperature. Moreover, the S-NPs have mostly disappeared at the benefit of the large ones (L-NPs) through some ripening effect. This was confirmed by DLS performed on the non-separated fresh and aged samples (figure 5) which shows a shift and narrowing of the size distributions towards the high values.

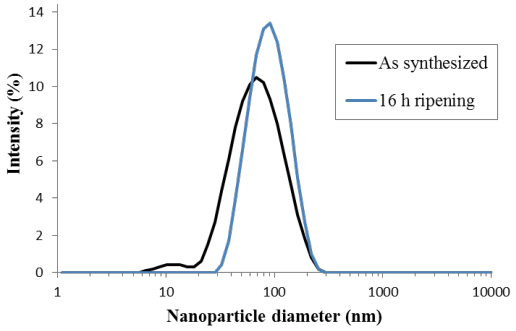

Figure 5: Evolution of non-separated nanoparticles, from fresh to aged samples (^{198}Au:Au NPs)

4 CONCLUSION

The suitability of plasma electrochemistry has been demonstrated for the rapid, efficient and on-site production of quality-controlled ^{198}Au doped nanoparticles for a next generation of brachytherapy procedures. The process presented, with its realtime synthesis monitoring by UV-Vis spectroscopy, is particularly adapted to automatisation and ease of operation with limited radiation exposure and contamination.

Acknowledgements: Mr Jean-François Sauvageau is acknowledged for his contribution to this manuscript.

5 REFERENCES

[1] Chanda, N *et al*., *Nanomedicine: Nanotechnology, Biology and Medicine* 2010, 6, 201-209.
[2] Bouchard, M *et al*., *Langmuir* 2015, 31, 7633-7643.
[3] Black, K. C. L *et al*., *ACS Nano* 2014, 8, 4385-4394.
[4] Jang, H. *et al*., *Biomaterials* 2013, 34, 3503-3510.
[5] Shou, Q. *et al*., *Journal of Colloid and Interface Science* 2011, 363, 481-489.
[6] Alkilany, A.*et al*., *Journal of Nanomaterials* 2015, 2015, Article ID 712359, 9 pages.